electronics

MDPI

Article

Numerical Calculation for the Line-of-Sight Attitudes of Multi-Address Transceivers without 2:1 Transmissions for Space Laser Communication Networking

Lihui Wang [1,2,3], Lizhong Zhang [1,3,4,*], Lixin Meng [1,3,4] and Yangyang Bai [1,3]

[1] School of Mechanical and Electrical Engineering, Changchun University of Science and Technology, Changchun 130022, China
[2] College of Engineering, Inner Mongolia University for Nationalities, Tongliao 028000, China
[3] Fundamental Science on Space-Ground Laser Communication Technology Laboratory, Changchun University of Science and Technology, Changchun 130022, China
[4] Peng Cheng Laboratory, Shenzhen 518055, China
* Correspondence: zlzcust@126.com

Abstract: In order to optimize space laser communication networking, the 2:1 transmissions for all reflectors on a multi-address transceiver can be removed. However, without the 2:1 transmissions, the reflectors exhibit doubled optical coupling effect in rotation, which reduces the numerical calculation precision of the attitudes of the reflectors' lines-of-sight (LOS). In the present study, using Snell's law of reflection and Euler's theorem, a mathematical model for the attitudes of the LOS of multiple reflectors without 2:1 transmissions was established, and a method was proposed for an indirect numerical calculation of the attitudes of the LOS by creating a Snell transformation matrix. This method eliminates the influence of the doubled optical coupling effect on the numerical solution of the line-of-sight attitudes of multi-reflectors. Compared to the direct numerical calculation method using the angular velocity, the calculation precisions achieved using the proposed method exhibited improvements of 3, 5, and 3 orders of magnitude in the three conical motions, respectively. The indirect calculation method and the numerical calculation model proposed in the present study, therefore, provide a theoretical basis for applying reflectors without 2:1 transmissions to multi-address transceivers.

Keywords: laser communication; without 2:1 transmissions; attitude of the LOS; snell transformation matrix

Citation: Wang, L.; Zhang, L.; Meng, L.; Bai, Y. Numerical Calculation for the Line-of-Sight Attitudes of Multi-Address Transceivers without 2:1 Transmissions for Space Laser Communication Networking. *Electronics* **2023**, *12*, 1575. https://doi.org/10.3390/electronics12071575

Academic Editor: Martin Reisslein

Received: 1 March 2023
Revised: 23 March 2023
Accepted: 25 March 2023
Published: 27 March 2023

1. Introduction

Space laser communication with high security, speed, and interference resistance has remained a focus of research in the field of communication globally [1]. In Telesat's "LEO constellation" program, SpaceX's "Starlink" program, and Amazon's "Kuiper" program, laser communication has been utilized as the major carrier of space communication network channels [2,3]. Therefore, developing a laser communication technology for a large-scale distributed cooperative network is considered a key approach to greatly improve 6G communication efficiency and bandwidth [4]. In America's space-based laser communication program (TSAT), global laser communication networking is realized through simultaneous laser communication of a high-orbit satellite and multiple low-orbit satellites [5]. In Japan's data relay satellite program (JDRS), the global communication network comprises a communication space that is divided into upper laser communication and lower microwave communication [6,7]. However, despite the specific schedules listed in the above programs, no follow-up reports have thus far been published. In China, our laboratory proposes to integrate a multi-reflector to realize the simultaneous laser communication of multi-LOS on the reflectors [8–10]. The prototype of the stated project has already been developed, and indoor networked laser communication has been realized.

In general, the gyros of a laser communication transceiver are mounted on the drive shafts of the reflectors to stabilize the LOS. In order to optimize the transceiver structure, a gyro is mounted on the base of a reflector while stabilizing all the LOS [11]. However, this modification requires a complicated mathematical model [12].

When the reflector rotates, there is a doubled optical coupling effect between the reflector and the line of sight, which seriously affects the accuracy of the attitude calculation of the LOS. Currently, in order to eliminate the doubled optical coupling effect, some companies and laboratories use the combination of an optical inertial reference unit (OIRU) and an Extended Corner Cube (ECC) [13–16]. However, the installation of this scheme is difficult, and the optical system is huge.

In another scheme, reflectors are mounted with 2:1 transmissions on the pitch axes to solve the problem of doubled optical coupling in the LOS stability of reflectors. This scheme leads to an increment in the volume and mass of the transceiver.

In order to optimize the transceiver of a space laser communication network, multi-reflectors without 2:1 transmissions are required for the simultaneous multi-address transmission of the data. However, reflectors without 2:1 transmissions result in a doubled optical coupling effect, due to which an ideal calculation result is not obtained by directly renewing the quaternion based on the angular velocity measured using gyros.

Using Snell's law of reflection, different studies [17–19] have systematically analyzed the doubled optical coupling effect of the LOS of reflectors without 2:1 transmissions and reported the mathematical model for this doubled optical coupling effect. However, few studies probe the numerical calculation of the developed model. Certain studies [20–24] have explored the modeling method for a real-time renewal of the carrier attitude in motion and reported a mathematical model for renewing the carrier attitude based on quaternion. In other studies [25,26], the calculation of a mathematical model for the carrier attitude has been discussed, and numerical calculation methods under several dynamic conditions have been provided. However, all these studies used a single carrier as the study object and probed less into attitude modeling and the calculation method for multi-carrier under dynamic conditions.

Based on the research of these references, according to the position relationships of the reflectors on a multi-address transceiver, we deduced the numerical solution model of the attitude of a multi-reflector through the Euler theorem. Then, according to the doubled optical coupling effect, we deduced the projection relationships between the reflector and the LOS in different coordinate systems and transformed the numerical solution of the reflector attitude into the numerical solution of the LOS attitude. Finally, under the typical conical motion, this indirect method and the direct calculation method of angular velocity were simulated, which verified the effectiveness and superiority of this indirect method.

The main contributions of this paper are summarized as follows:

(1) A new method of establishing a reflector coordinate system is proposed, which realizes the conversion of projections between a reflector and LOS in different coordinate systems.
(2) A mathematical method for the mutual conversion between the attitudes of a multi-reflector is proposed, which can realize the numerical solution of the attitudes of a reflector and the LOS at any position. The attitude of all the reflectors and the LOS can be calculated simultaneously by a single gyro.
(3) According to the spatial transformation relation of Snell's law of reflection, the Snell transformation matrix is established. Through the Snell transformation of LOS in different reflector coordinate systems, the doubled coupling effects produced in the numerical solution of the LOS attitude of a multi-reflector are eliminated.

The rest of this article is organized as follows. The principle of laser communication networking and the working mode of a multi-access optical transceiver without 2:1 transmissions are presented in Section 2. The numerical solution model and numerical methods are studied in Section 3, and comparative simulation experiments on the numerical solution of the LOS attitude of six reflectors are studied in Section 4. Finally, the main conclusions are drawn in Section 5.

2. Scheme for Space Laser Communication Networking

2.1. Networking Principle

The networking of the space laser communication links requires the creation of spacecraft relay communication nodes. GEO satellites with wide coverage are treated as the relay communication nodes for realizing real-time laser communication with ground stations, LEO satellites, spacecraft, and space stations, thereby forming an all-encompassing laser communication network with multi-node. A space laser communication networking structure is depicted in Figure 1.

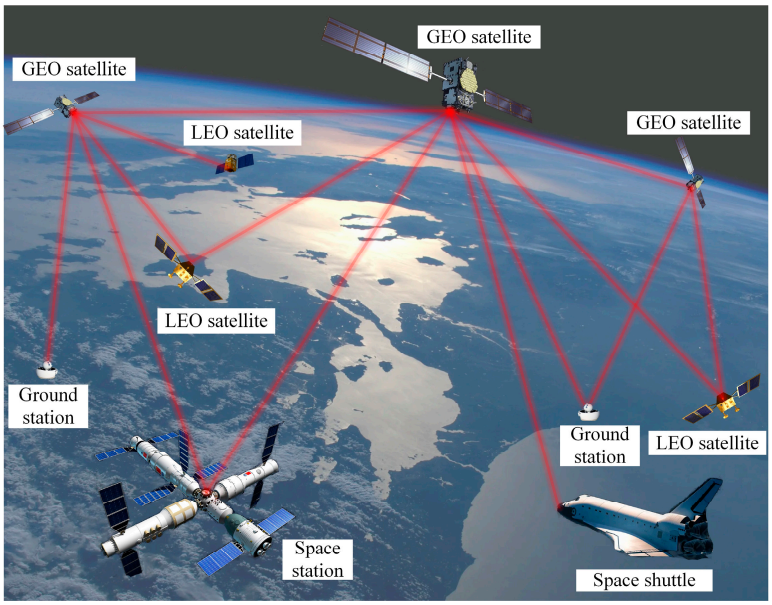

Figure 1. The illustration of a space laser communication networking structure.

2.2. Indoor Experiment for Laser Communication Networking

An experimental system was designed for laser communication networking. The system was established based on the characteristics of such networking. The developed system comprised one master optical transceiver and four slave optical transceivers. The master optical transceiver was placed in the room center and could communicate with the four slave optical transceivers simultaneously. The slave optical transceivers were placed around the master optical transceiver and simulated in horizontal, vertical, 45°, and –45° motions on a slideway (Figure 2).

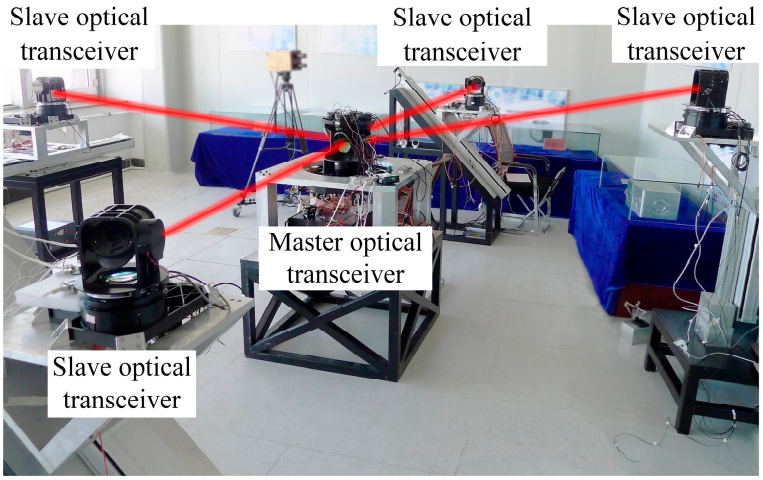

Figure 2. The illustration of the indoor experiment for laser communication networking.

In the experiment, the four slave optical transceivers were in different rectilinear motion states and scanned the beacon beam of the master optical transceiver. The master optical transceiver has four reflectors that stare at the approximate positions of the slave transceivers, waiting for the beacon beams from the slave optical transceivers. Once the beacon beams from the slave optical transceivers were captured, the master transceiver sent a confirmation beacon beam to the slave optical transceivers and adjusted the four reflectors to ensure the simultaneous communication of the four laser paths. Accordingly, the simultaneous siting, capture, and tracking of the four points were realized in this experiment. The actual master optical transceiver and slave optical transceivers are depicted in Figure 3.

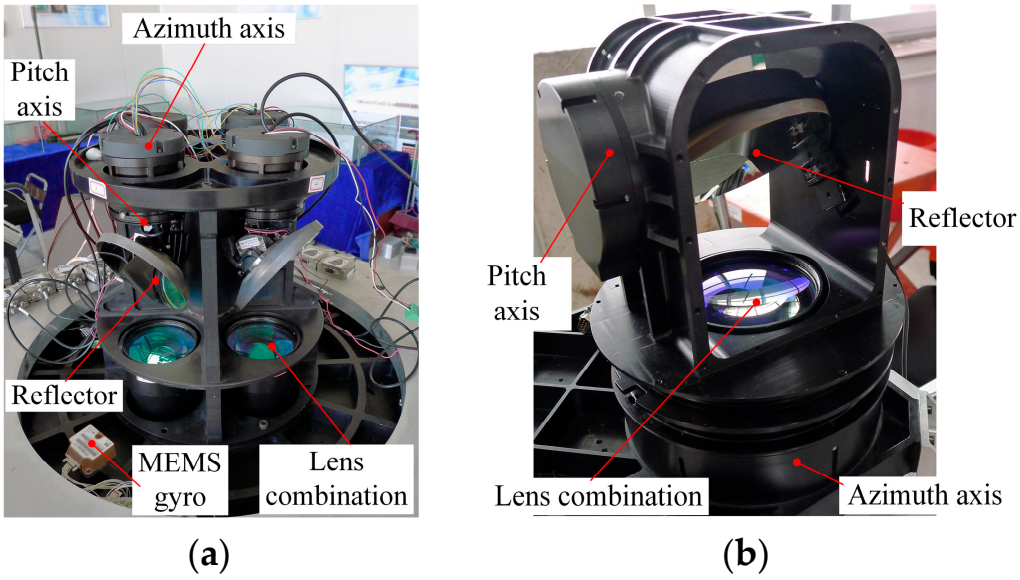

Figure 3. Transceivers for indoor laser communication networking. (**a**) The master optical transceiver; (**b**) The slave optical transceivers.

Four reflectors were mounted around the master optical transceiver. The reflectors and the azimuth-pitch frameworks together form a coarse tracking system for regulating the attitudes of the LOS of the reflectors. A MEMS gyro was mounted on the base of the master transceiver to stabilize the LOS of each reflector. The structures of the slave transceivers were the same as that of the master transceiver. The optical lenses of the two types of transceivers formed a telescoping system to facilitate the collective detection of the parallel beacon beams and the parallel emission of the beacon light source.

2.3. Multi-Reflector Scheme for Laser Communication Networking

With advancements in laser communication network technology, the requirements for the quantity and positions of reflectors on multi-address transceivers have been increasing. In order to embody the universality of the proposed LOS stabilization method, in the model transceiver six reflectors were distributed annularly in two layers, one above the other, as illustrated in Figure 4.

Figure 4a,b depict the multi-address transceivers comprising six reflectors. In order to achieve the simultaneous operation of six clear apertures, the reflectors were distributed in two layers, one above the other (three reflectors in each layer), and had their specific optical paths. Figure 4a depicts the multi-address transceiver with 2:1 transmissions, where each reflector had a 2:1 transmission which weakened the doubled optical coupling effect. Figure 4b depicts the multi-address transceivers without 2:1 transmissions, where the attitudes of the LOS of the reflectors were controlled directly using a motor.

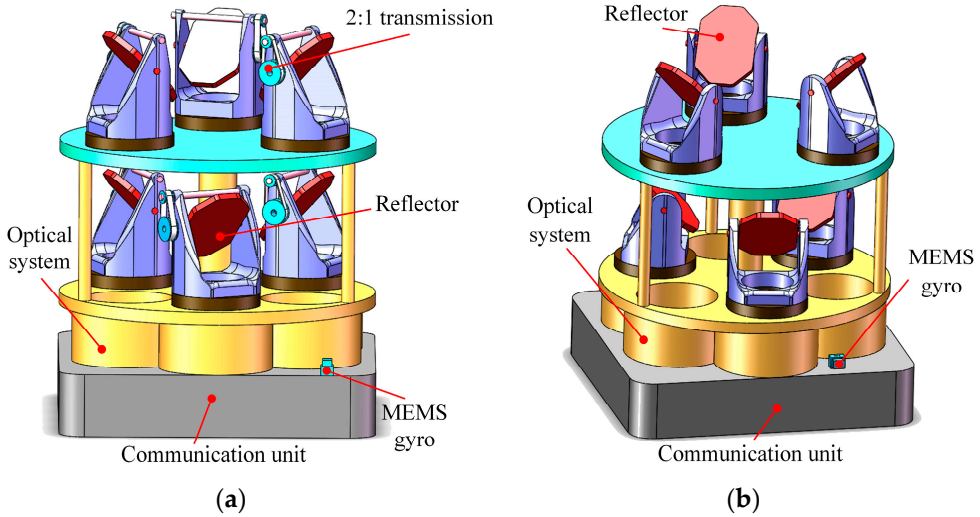

Figure 4. An illustration of the different types of multi-address transceivers. (**a**) Transceiver with 2:1 transmissions; (**b**) Transceiver without 2:1 transmissions.

3. Calculations for the Attitudes of the LOS of the Multi-Reflectors

3.1. Establishing the Coordinate System

The base's coordinate system $O_{4\times4}Y_4Z_4$ was established such that it coincided with the initial azimuth axis, pitch axis, and roller of the base. The barycenter of the base was the origin of this system. The coordinate system coinciding with the coordinate system of the base when the multi-address transceivers were in their initial steady states was defined as the reference coordinate system $OX_1Y_1Z_1$. When the base's coordinate system moved, the reference coordinate system was considered the static coordinate system to measure the rotation Euler angle of the base's coordinate system.

According to the positioning characteristics of the six reflectors' coordinate axes, the six reflectors' coordinate systems $O_{4i}X_{4i}Y_{4i}Z_{4i}$ (i = 1,2, . . . ,6) were established on two parallel planes, one for each of the three coordinate systems. The coordinate system $O_4X_4Y_4Z_4$ rotated for 0°, 60°, 120°, 180°, 240°, and 300°, respectively, around the Z_4 axis, thereby transforming into six coordinate systems, namely, $O_{41}X_{41}Y_{41}Z_{41}$, $O_{42}X_{42}Y_{42}Z_{42}$, $O_{43}X_{43}Y_{43}Z_{43}$, $O_{44}X_{44}Y_{44}Z_{44}$, $O_{45}X_{45}Y_{45}Z_{45}$, and $O_{46}X_{46}Y_{46}Z_{46}$. The transformed coordinate systems of each reflector are illustrated in Figure 5.

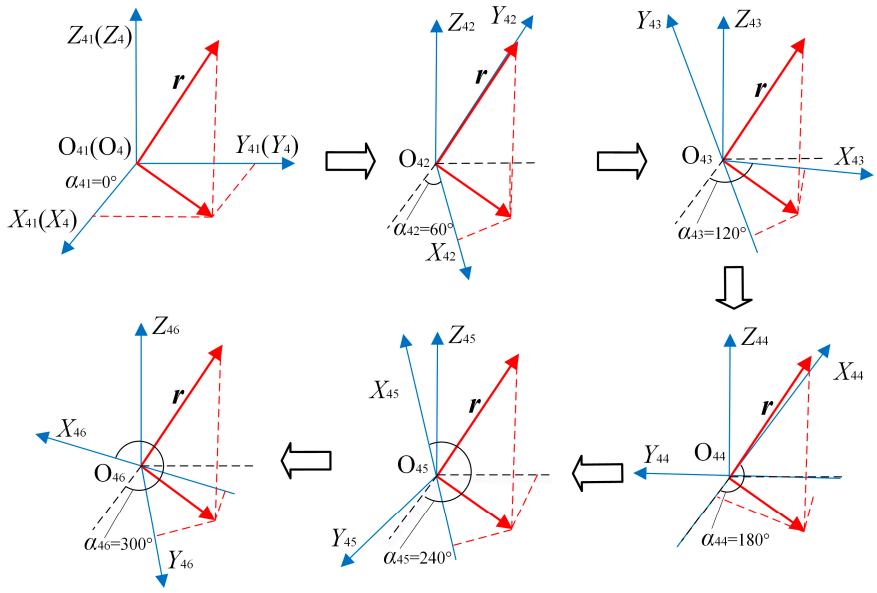

Figure 5. The illustration of the transformation of the multi-reflector's coordinate systems.

A spatial vector $\boldsymbol{n}$ was established coinciding with the initial position of a reflector's LOS. When the coordinate system rotated in space, the projections of the said vector $\boldsymbol{n}$ were observed in different coordinate systems. Accordingly, the attitude angles of the vector $\boldsymbol{n}$ in different coordinate systems were calculated. Further, the reflector's attitude could be adjusted according to the calculated attitude angles of the LOS.

3.2. Mathematical Model of the Attitudes of the LOS of the Multi-Reflector

Let $\boldsymbol{r}_1$ be the projection of the initial vector $\boldsymbol{n}$ in the reference coordinate system $OX_1Y_1Z_1$ and $\boldsymbol{r}_{41}$ be the projection of the initial vector $\boldsymbol{n}$ in the reflector coordinate system $O_{41}X_{41}Y_{41}Z_{41}$. Then, when the reference coordinate system $OX_1Y_1Z_1$ rotated for an angle α around the axis Z_1, a transformed coordinate system $O_2X_2Y_2Z_2$ was obtained, with the transformation matrix $\boldsymbol{C}_1^2$. When the coordinate system $O_2X_2Y_2Z_2$ rotated for an angle β around its axis Y_2, a coordinate system $OX_3Y_3Z_3$ was obtained, with the transformation matrix $\boldsymbol{C}_2^3$. When the coordinate system $O_3X_3Y_3Z_3$ rotated for an angle γ around the axis Y_3 of the reference coordinate system, a coordinate system $OX_4Y_4Z_4$ (which is the coordinate system of the base) was obtained, with the transformation matrix $\boldsymbol{C}_3^4$. Accordingly, the transformation matrix $\boldsymbol{C}_1^4$ from the reference coordinate system to the base's coordinate system was as follows:

$$\boldsymbol{C}_1^4 = \boldsymbol{C}_3^4\boldsymbol{C}_2^3\boldsymbol{C}_1^2 \tag{1}$$

The above transformation matrix could be expressed in the form of a direction cosine matrix, as follows:

$$\boldsymbol{C}_1^4 = [\boldsymbol{C}_4^1]^T \tag{2}$$

where $\boldsymbol{C}_1^4$ is the attitude matrix of the vector in the reflector coordinate system $O_{41}X_{41}Y_{41}Z_{41}$. Accordingly, the direction cosine transformation relationship between $\boldsymbol{r_1}$ and $\boldsymbol{r_4}$ was as follows:

$$\boldsymbol{r}_4 = \boldsymbol{C}_4^1\boldsymbol{r}_1 \tag{3}$$

When the coordinate system of the base rotated six times around the Z axis, six reflector coordinate systems were obtained. Let α_i be the rotation angle and i be the serial number of the corresponding reflector. Then, the following is obtained:

$$\boldsymbol{C}_4^i = \begin{bmatrix} \cos\alpha_{\mathrm{i}} & \sin\alpha_{\mathrm{i}} & 0 \\ -\sin\alpha_i & \cos\alpha_i & 0 \\ 0 & 0 & 1 \end{bmatrix} \tag{4}$$

where $\boldsymbol{C}_4^i$ is the LOS attitude transformation matrix for the transition from the base's coordinate system to the reflector coordinate systems. Let $\boldsymbol{r}_{4i}$ be the vector of each reflector's LOS. Then, the LOS vector of a reflector without a 2:1 transmission was indicated as follows:

$$\boldsymbol{r}_{4i} = \boldsymbol{C}_4^i\boldsymbol{r}_4 \tag{5}$$

Substituting Formula (3) into Formula (5), the following formula was obtained:

$$\boldsymbol{r}_{4i} = \boldsymbol{C}_4^i\boldsymbol{C}_4^1\boldsymbol{r}_1 \tag{6}$$

where

$$\boldsymbol{r}_1 = \begin{bmatrix} x_1 \\ y_1 \\ z_1 \end{bmatrix}, \boldsymbol{r}_4 = \begin{bmatrix} x_4 \\ y_4 \\ z_4 \end{bmatrix}, \boldsymbol{r}_{4i} = \begin{bmatrix} x_{4i} \\ y_{4i} \\ z_{4i} \end{bmatrix} \tag{7}$$

In each reflector coordinate system, the azimuth and pitching attitude of the reflector can be expressed as

$$\alpha_{\mathrm{L}} = \arctan\left(\frac{y_{4i}}{x_{4i}}\right) \tag{8}$$

$$\beta_{\mathrm{L}} = \arcsin\left(\frac{z_{4i}}{\sqrt{x_{4i}^2 + y_{4i}^2}}\right) \tag{9}$$

When the multi-address transceivers were mounted with the reflectors without 2:1 transmissions, doubled optical coupling effect appeared in the rotation of the pitch axis, as illustrated in Figure 6.

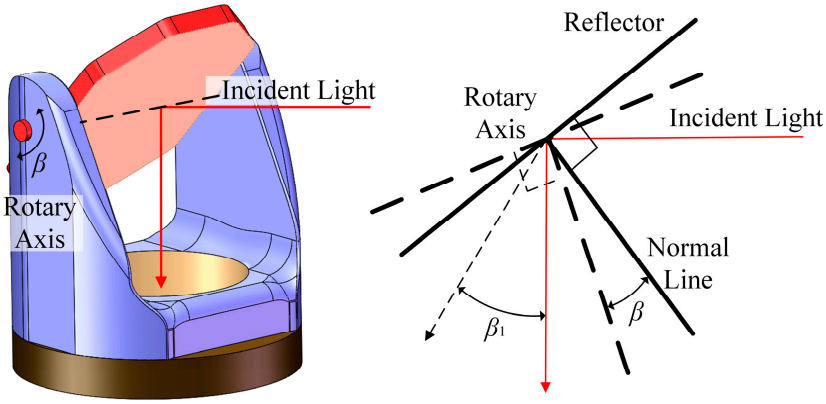

Figure 6. The double optical coupling principle of the light paths of the reflectors.

According to Snell's law of reflection, when a reflector rotates for an angle β, its LOS rotates for an angle β_1. Accordingly, the geometrical relationship between the two angles is:

$$\beta_1 = 2\beta_{\mathrm{L}} \tag{10}$$

β_1 is the LOS attitude of each reflector. In order to eliminate the doubled optical coupling effect, we need to establish a reflector coordinate system with a double LOS. The vector $\boldsymbol{r}_{4i}$ in six reflector coordinate systems is projected into the reflector coordinate system with double LOS to obtain the vector $\boldsymbol{r}_{4i}^1$. According to Euler's theorem and Snell's law of reflection, the transformation matrix between the two coordinate systems is established.

$$\boldsymbol{C}_4^2 = \begin{bmatrix} \cos\beta_1 & 0 & -\sin\beta_1 \\ 0 & 1 & 0 \\ \sin\beta_1 & 0 & \cos\beta_1 \end{bmatrix} \tag{11}$$

where $\boldsymbol{C}_4^2$ is the Snell transformation matrix representing a projection transformation relationship between the LOS of the reflectors with and without 2:1 transmissions. Then, the following relationship would be obtained:

$$\boldsymbol{r}_{4\mathrm{i}}^1 = \boldsymbol{C}_4^2 \boldsymbol{r}_{4\mathrm{i}} \tag{12}$$

where $\boldsymbol{r}_{4i}^1$ is the attitude vector of the LOS calculated indirectly based on the Snell transformation matrix.

3.3. Numerical Calculations for the Attitudes of the LOS of the Multi-Reflector

3.3.1. Quaternion-Based Numerical Calculation Model

The angular velocity was measured using MEMS gyros, and the quaternion matrix was used for calculating $\boldsymbol{C}_4^1$ numerically. The quaternion was assumed to be as follows:

$$\boldsymbol{q} = \lambda + q_1\boldsymbol{i} + q_2\boldsymbol{j} + q_3\boldsymbol{k} \tag{13}$$

where λ, q_1, q_2, and q_3 are real numbers, while $\boldsymbol{i}$, $\boldsymbol{j}$, and $\boldsymbol{k}$ are unit vectors for the different directions in three dimensions.

The transformation relationship between $\boldsymbol{r}_1$ and $\boldsymbol{r}_4$ could be expressed in the form of quaternion, as follows:

$$\boldsymbol{r}_1 = \boldsymbol{q}^{-1}\boldsymbol{r}_4\boldsymbol{q} \tag{14}$$

Substituting Formula (13) into Formula (14), the following formula is obtained:

$$\boldsymbol{r}_1 = \boldsymbol{C}'\boldsymbol{r}_4 \tag{15}$$

where

$$\boldsymbol{C}' = \begin{bmatrix} \lambda^2 + q_1^2 - q_2^2 - q_3^2 & 2(q_1q_2 + \lambda q_3) & 2(q_1q_3 - \lambda q_2) \\ 2(q_1q_2 - \lambda q_3) & \lambda^2 + q_2^2 - q_1^2 - q_3^2 & 2(q_2q_3 + \lambda q_1) \\ 2(q_1q_3 + \lambda q_2) & 2(q_2q_3 - \lambda q_1) & (\lambda^2 + q_3^2 - q_1^2 - q_2^2) \end{bmatrix} \tag{16}$$

$\boldsymbol{C}'$ represents the quaternion transformation matrix, which was transformed into a transformation matrix from $\boldsymbol{r}_4$ to $\boldsymbol{r}_1$, such that the following holds:

$$\boldsymbol{C}_4^1 = (\boldsymbol{C}')^T \tag{17}$$

Next, the quaternion-based differential equations were obtained, generating the attitude matrix of the LOS. The quaternion-based rotation equation was as follows:

$$\dot{\boldsymbol{q}} = \frac{1}{2}\boldsymbol{q}\boldsymbol{\omega} \tag{18}$$

where $\boldsymbol{\omega}$ is the angular velocity of the base disturbance measured using a MEMS gyro.

$$\boldsymbol{\omega} = \begin{bmatrix} \omega_x \\ \omega_y \\ \omega_z \end{bmatrix} \tag{19}$$

The equations were resolved through iteration with the fourth-order Runge–Kutta (RK4) method, as follows:

$$\begin{cases} K_1 = \frac{\mathrm{T}}{2}\boldsymbol{q}(t)\boldsymbol{\omega}(t) \\ K_2 = \frac{\mathrm{T}}{2}[\boldsymbol{q}(t) + \frac{K_1}{2}][\boldsymbol{\omega}(t + \frac{\mathrm{T}}{2})] \\ K_3 = \frac{\mathrm{T}}{2}[\boldsymbol{q}(t) + \frac{K_2}{2}][\boldsymbol{\omega}(t + \frac{\mathrm{T}}{2})] \\ K_4 = \frac{\mathrm{T}}{2}[\boldsymbol{q}(t) + K_3][\boldsymbol{\omega}(t + \mathrm{T})] \\ \boldsymbol{q}(t + \mathrm{T}) = \boldsymbol{q}(t) + \frac{\mathrm{T}}{6}(K_1 + 2K_2 + 2K_3 + K_4) \end{cases} \tag{20}$$

where K_1, K_2, K_3, and K_4 are the intermediate variables of the applied iteration algorithm, T is the step size of the system, $\boldsymbol{\omega}(t)$ denotes the real-time angular velocity measured and updated using gyros, $\boldsymbol{q}$(t) represents the real-time calculation data of the quaternion at time t, and $\boldsymbol{q}(t$ + T) is the quaternion generated through iteration using the stated algorithm at the next time.

3.3.2. Direct Calculation Method

In practice, the angular velocities measured by the gyros are generally used for updating the quaternion. Considering that the pitch angle was transformed into a doubled relationship directly during the modeling of the doubled optical coupling effect, the angular velocity relationship was also transformed into a doubled relationship directly, as follows:

$$\omega_y = 2\omega_y^1 \tag{21}$$

where ω_{y}^1 denotes the angular velocity perceived by the gyros, namely the rotating angular velocity of the reflector, and ω_y is the rotating angular velocity of the LOS. Substituting Formula (21) into Formula (20) for the numerical iteration would then generate the quaternion updated in real-time. In this manner, the attitude of the reflector's LOS was calculated.

4. Simulation Experiment

According to the verification requirement of the strap-down inertial navigation system for the numerical attitude renewal algorithm, three typical conical motions were selected as the ideal reference inputs for the multi-address transceivers [27]. Provided that the base's coordinate system $O_4X_4Y_4Z_4$ coincided with the reference coordinate system, during the rotation of the former coordinate system for an angle a around Y_1, its axis X_4 and the axis X_1 of the latter coordinate system formed an included angle, which was the cone angle a of the conical motion. At this time, axis X4 was the sideline OL of the conical motion. The base's coordinate system $O_4X_4Y_4Z_4$ rotated around the axis X_1 at an angular velocity ω, and the step size for the calculation was h. The equivalent unit vector of this conical motion was as follows:

$$\boldsymbol{u}_L^R = \begin{bmatrix} 0 \\ \cos \omega t \\ \sin \omega t \end{bmatrix} \tag{22}$$

Accordingly, the quaternion from the base's coordinate system to the reference coordinate system was as follows:

$$\boldsymbol{Q}(t) = \begin{bmatrix} \cos \frac{a}{2} \\ 0 \\ \sin \frac{a}{2} \cos \omega t \\ \sin \frac{a}{2} \sin \omega t \end{bmatrix} \tag{23}$$

The angular velocity vector of the conical motion of the base's coordinate system relative to the reference coordinate system was as follows:

$$\boldsymbol{\omega}(t) = \begin{bmatrix} -2\omega \sin^2 \frac{a}{2} \\ -\omega \sin a \sin \omega t \\ \omega \sin a \cos \omega t \end{bmatrix} \tag{24}$$

The simulation lasted for 100 s, and the step size h was 0.05 s. Using the RK4 numerical calculation method, the calculation error curves were obtained for the attitudes of the LOS of the stated six reflectors in the coordinate systems $O_{41}X_{41}Y_{41}Z_{41}$, $O_{42}X_{42}Y_{42}Z_{42}$, $O_{43}X_{43}Y_{43}Z_{43}$, $O_{44}X_{44}Y_{44}Z_{44}$, $O_{45}X_{45}Y_{45}Z_{45}$, and $O_{46}X_{46}Y_{46}Z_{46}$. We obtained the LOS attitude curves and calculation error curves of six reflectors under the ideal conical motion, as shown in Figures 7–18.

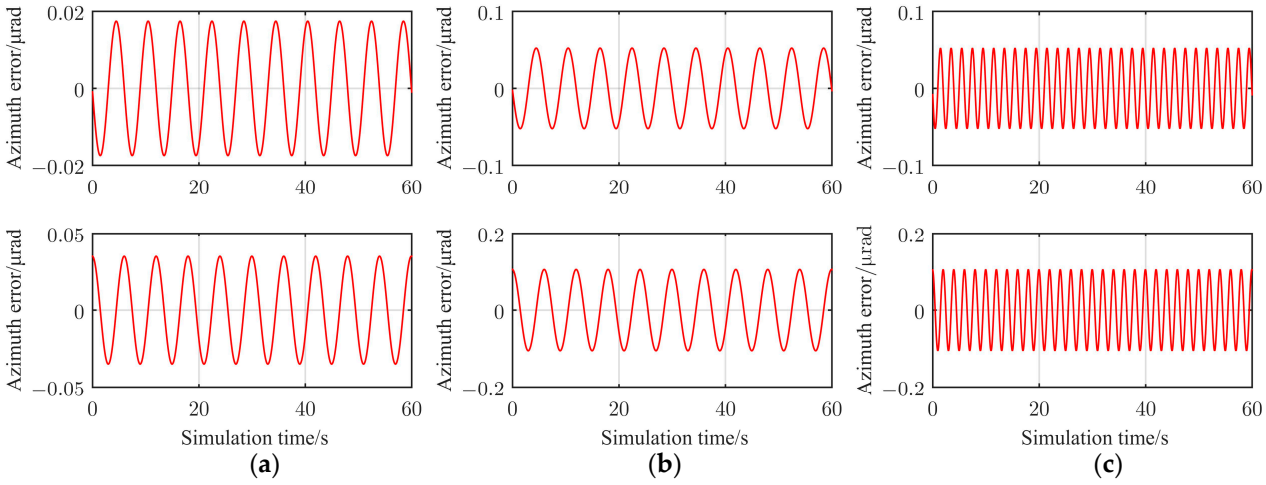

Figure 7. The LOS attitude curves under the condition of conical motion in an ideal state in the reflector coordinate system $O_{41}X_{41}Y_{41}Z_{41}$. (**a**) $a = 1°$, $\omega = 60°/s$; (**b**) $a = 3°$, $\omega = 60°/s$; (**c**) $a = 1°$, $\omega = 180°/s$.

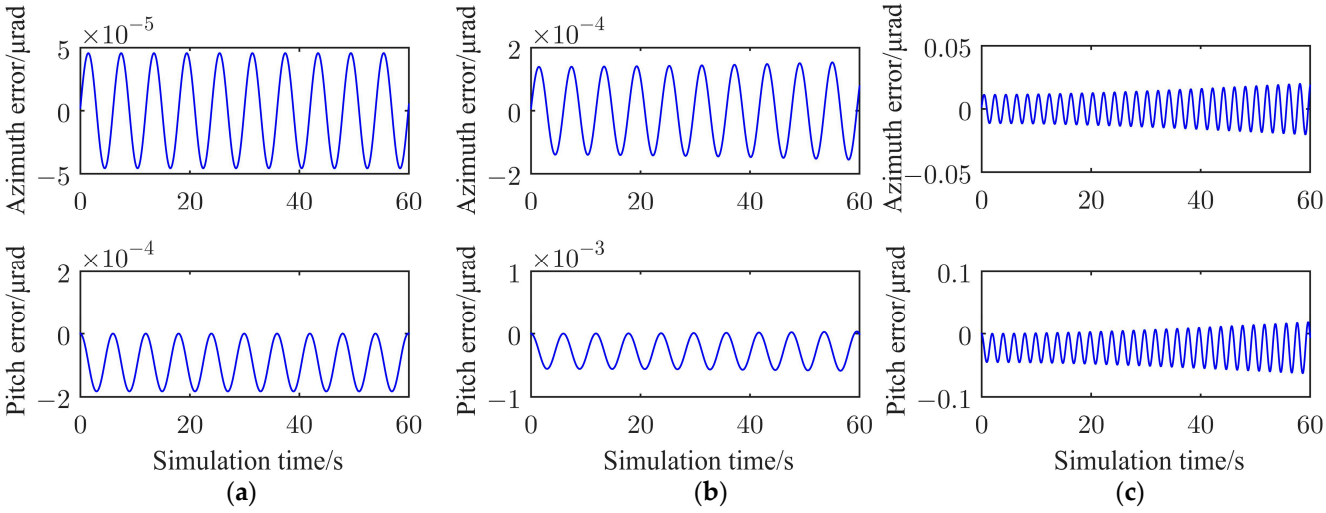

Figure 8. The error curve of the calculation of the indirect numerical calculation method in the reflector coordinate system $O_{41}X_{41}Y_{41}Z_{41}$. (**a**) $a = 1°$, $\omega = 60°/s$; (**b**) $a = 3°$, $\omega = 60°/s$; (**c**) $a = 1°$, $\omega = 180°/s$.

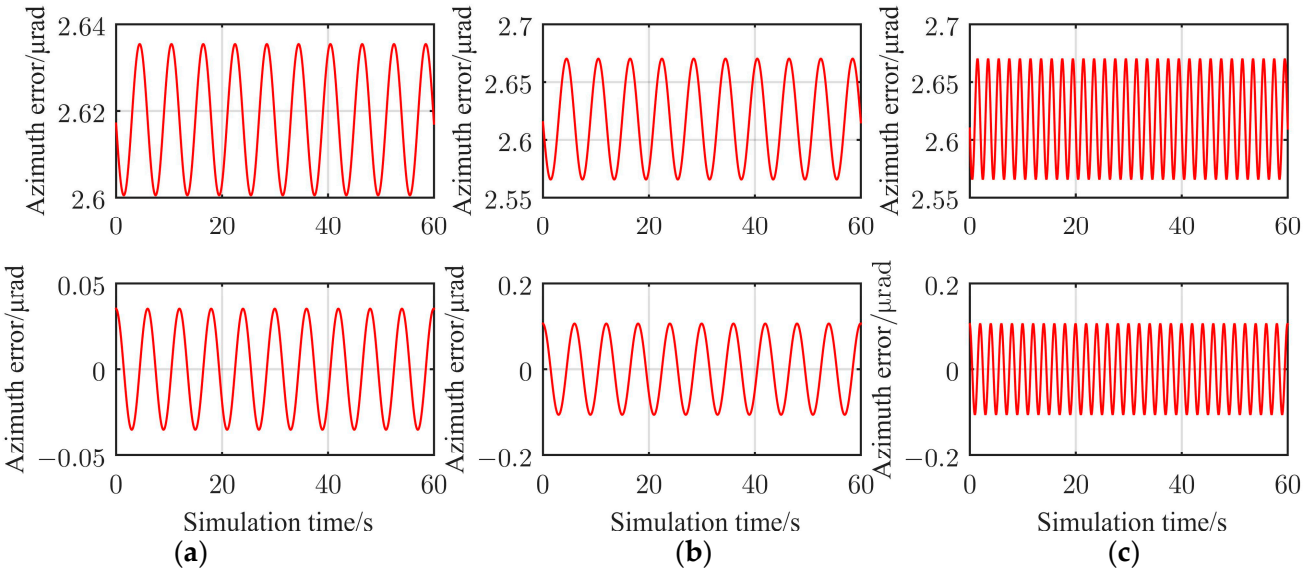

Figure 9. The LOS attitude curves under the condition of conical motion in an ideal state in the reflector coordinate system $O_{42}X_{42}Y_{42}Z_{42}$. (**a**) $a = 1°$, $\omega = 60°/s$; (**b**) $a = 3°$, $\omega = 60°/s$; (**c**) $a = 1°$, $\omega = 180°/s$.

As revealed, Figures 7, 9, 11, 13, 15 and 17 show the LOS attitude curves of six reflectors under the condition of conical motion in an ideal state. As the cone angle a and the angular speed ω increase, the motion environment becomes increasingly harsh. The azimuth and pitch curves are constant in amplitude and periodic. Although the amplitude of the curve is not large, great fluctuations appear at the peak and valley. When conducting numerical resolution for the attitude of LOS, because the RK4 method is an equal step method, it is difficult to realize numerical approximation in detail near the peak and valley. This method uses the angular speed of the gyro, so a certain compensation can be done at the peak and valley. Figures 8, 10, 12, 14, 16 and 18 show the resolution error curves of LOS attitude corresponding to the reflectors. We can see from the curves that the resolution errors at the peak and valley are large and the error curves show periodicity. Although the indirect method shows high precision in terms of resolution, error accumulations of different levels occur in the coordinate systems of the six reflectors, which do not result in

too large deviations in the error curve. The numerical calculation error curves obtained using the indirect calculation method for the six reflector coordinate systems were different. The calculation errors increased with the increments in the simulation duration, cone angle a, and angular velocity ω. The determined numerical calculation error values are listed in Table 1.

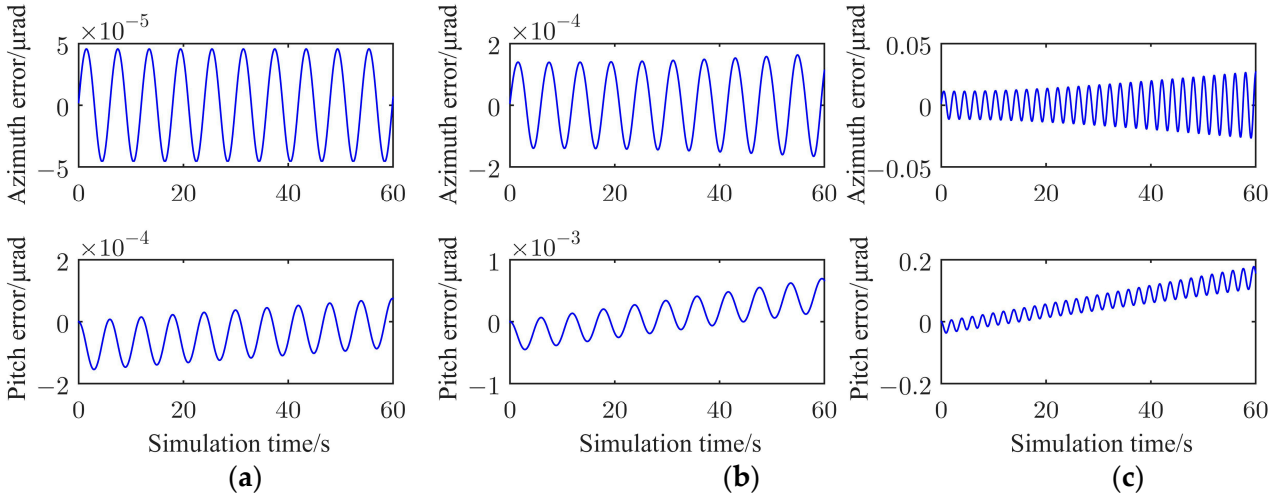

Figure 10. The error curve of the calculation of the indirect numerical calculation method in the reflector coordinate system $O_{42}X_{42}Y_{42}Z_{42}$. (**a**) $a = 1°$, $\omega = 60°/s$; (**b**) $a = 3°$, $\omega = 60°/s$; (**c**) $a = 1°$, $\omega = 180°/s$.

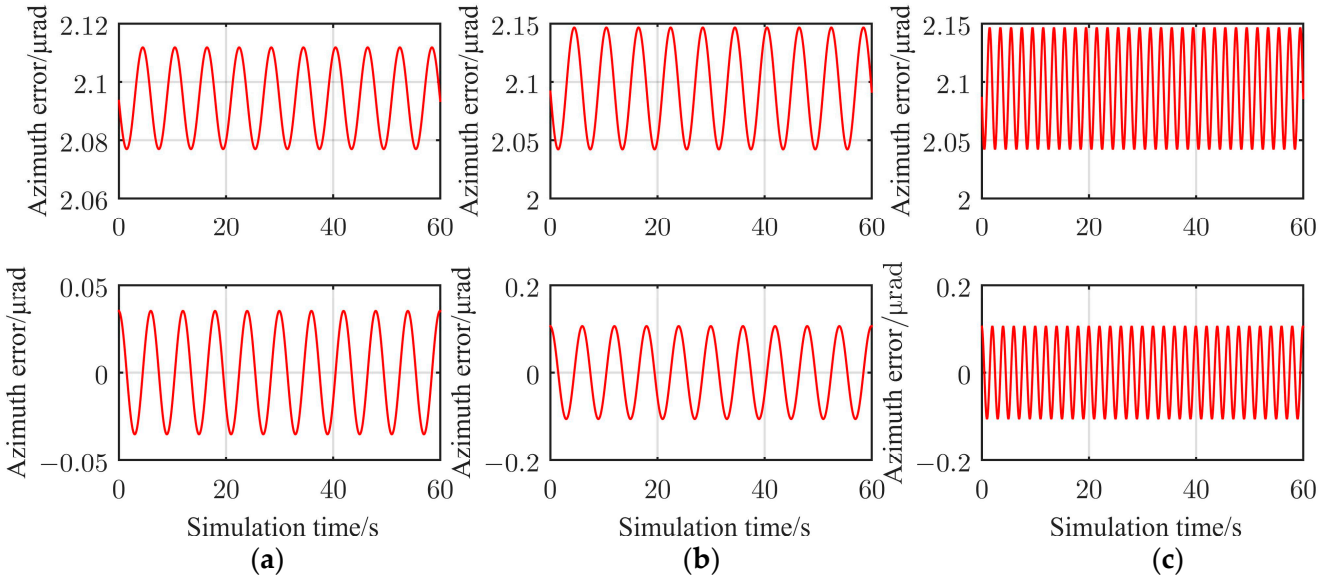

Figure 11. The LOS attitude curves under the condition of conical motion in an ideal state in the reflector coordinate system $O_{43}X_{43}Y_{43}Z_{43}$. (**a**) $a = 1°$, $\omega = 60°/s$; (**b**) $a = 3°$, $\omega = 60°/s$; (**c**) $a = 1°$, $\omega = 180°/s$.

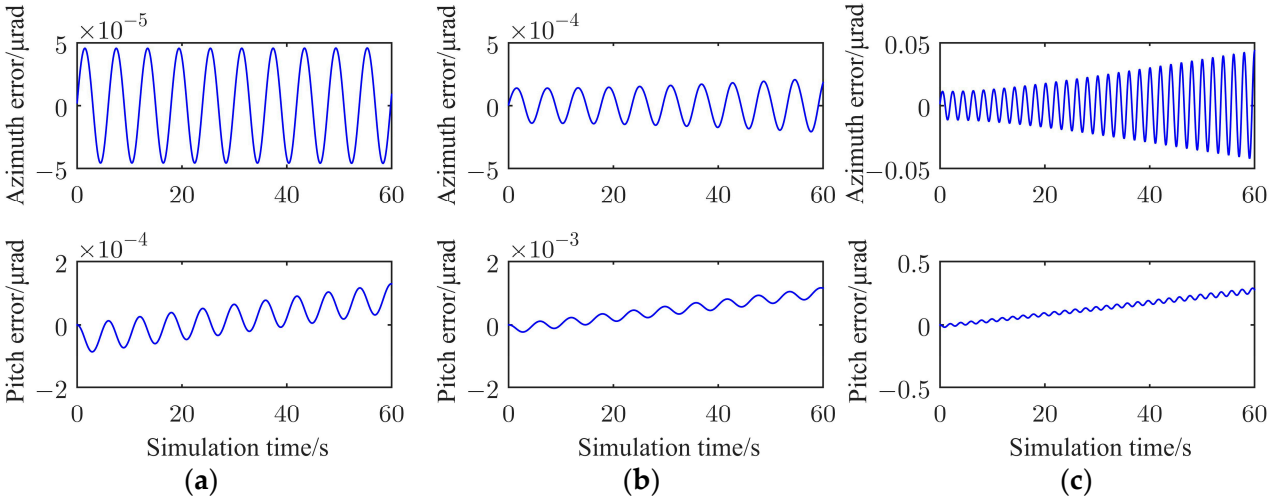

Figure 12. The error curve of the calculation of the indirect numerical calculation method in the reflector coordinate system $O_{43}X_{43}Y_{43}Z_{43}$. (**a**) $a = 1°$, $\omega = 60°/s$; (**b**) $a = 3°$, $\omega = 60°/s$; (**c**) $a = 1°$, $\omega = 180°/s$.

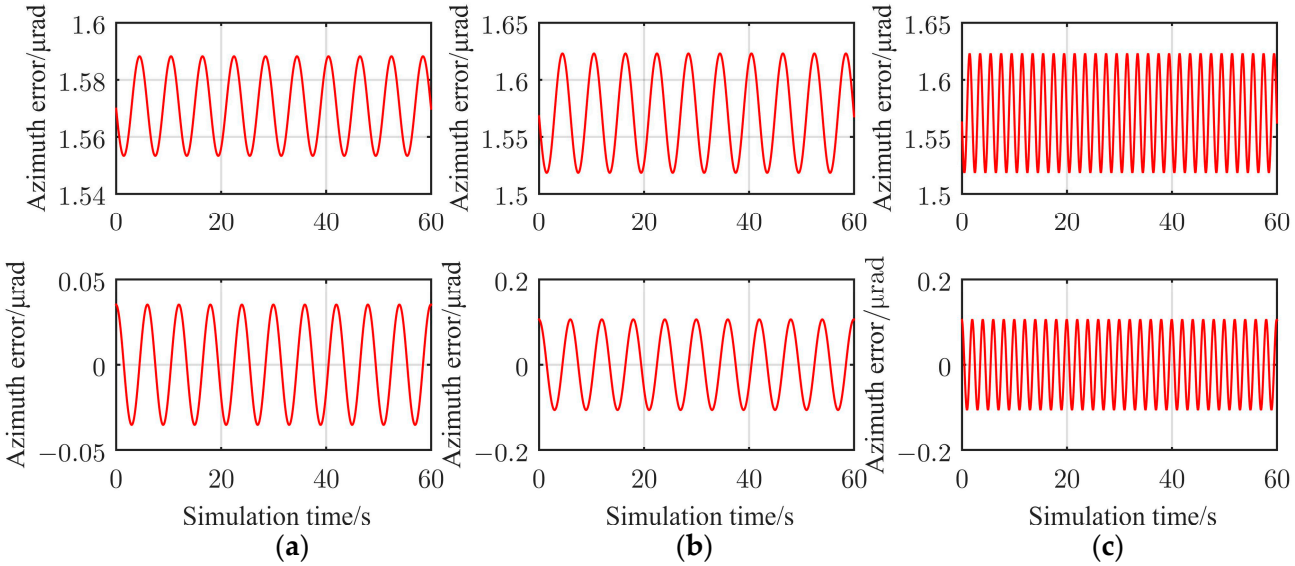

Figure 13. The LOS attitude curves under the condition of conical motion in an ideal state in the reflector coordinate system $O_{44}X_{44}Y_{44}Z_{44}$. (**a**) $a = 1°$, $\omega = 60°/s$; (**b**) $a = 3°$, $\omega = 60°/s$; (**c**) $a = 1°$, $\omega = 180°/s$.

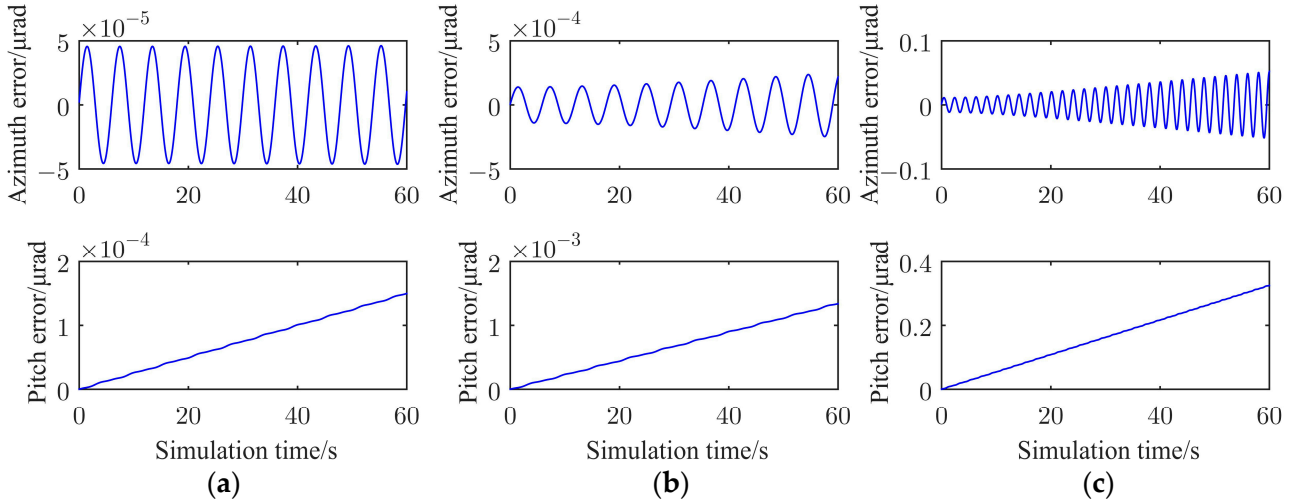

Figure 14. The error curve of the calculation of the indirect numerical calculation method in the reflector coordinate system $O_{44}X_{44}Y_{44}Z_{44}$. (**a**) $a = 1°$, $\omega = 60°/s$; (**b**) $a = 3°$, $\omega = 60°/s$; (**c**) $a = 1°$, $\omega = 180°/s$.

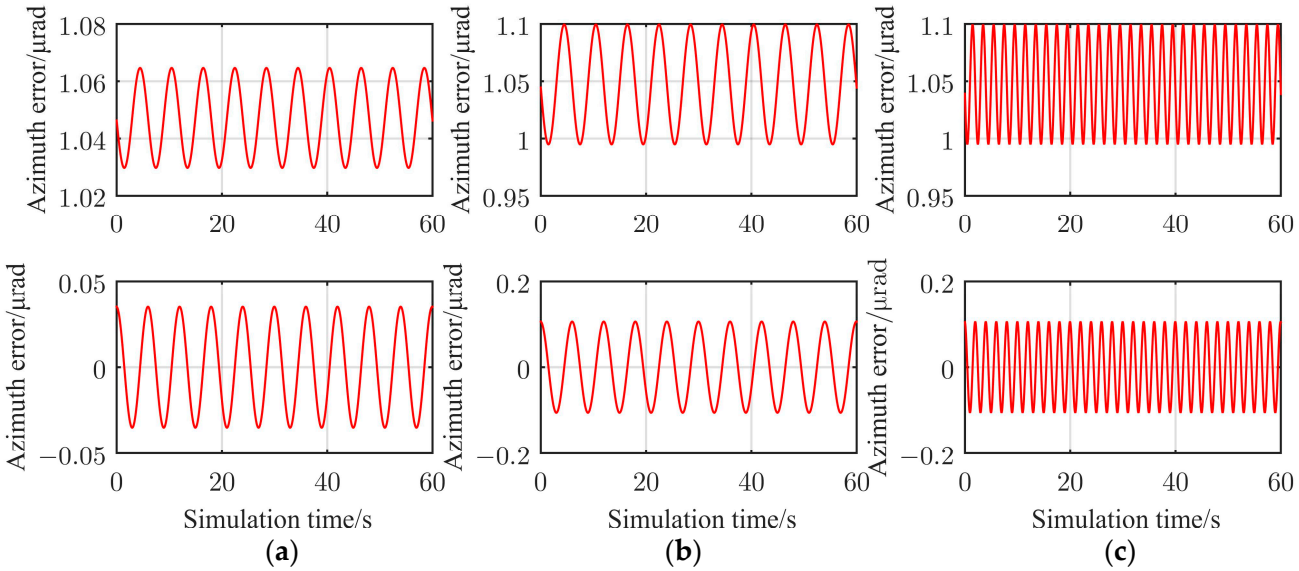

Figure 15. The LOS attitude curves under the condition of conical motion in an ideal state in the reflector coordinate system $O_{45}X_{45}Y_{45}Z_{45}$. (**a**) $a = 1°$, $\omega = 60°/s$; (**b**) $a = 3°$, $\omega = 60°/s$; (**c**) $a = 1°$, $\omega = 180°/s$.

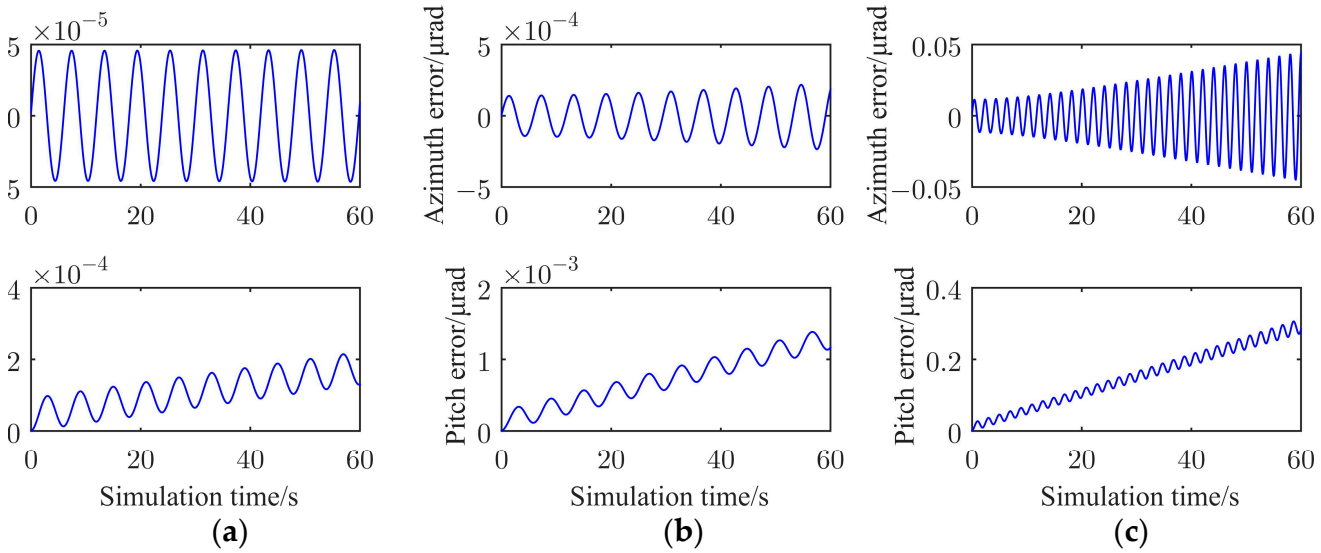

Figure 16. The error curve of the calculation of the indirect numerical calculation method in the reflector coordinate system $O_{45}X_{45}Y_{45}Z_{45}$. (**a**) $a = 1°$, $\omega = 60°/s$; (**b**) $a = 3°$, $\omega = 60°/s$; (**c**) $a = 1°$, $\omega = 180°/s$.

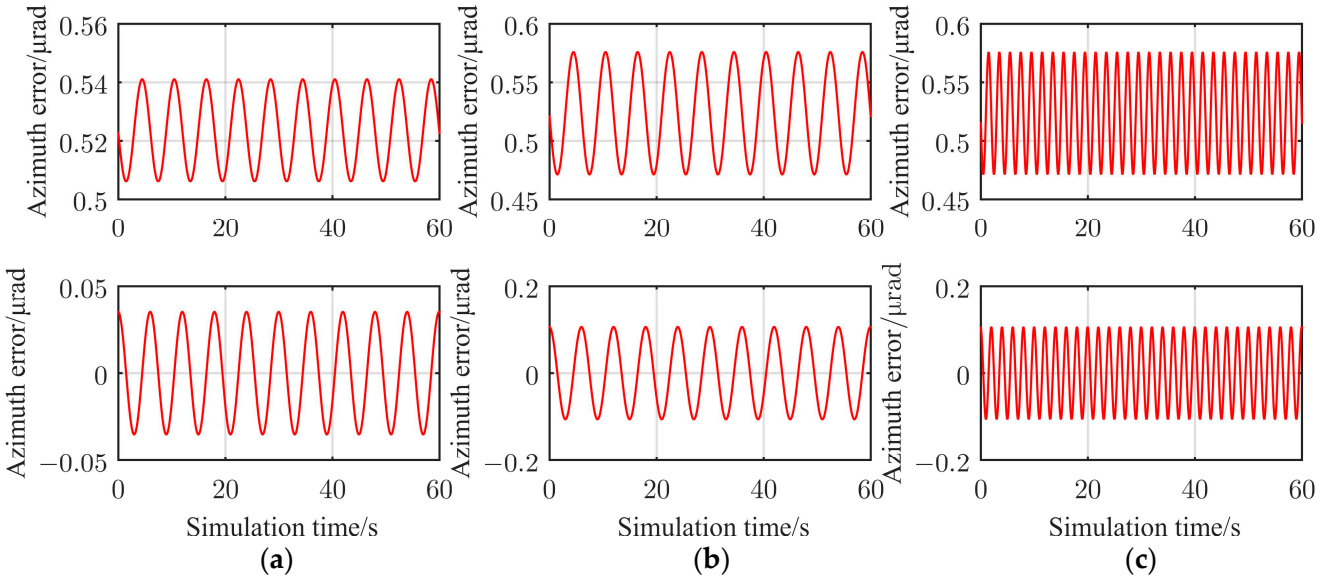

Figure 17. The LOS attitude curves under the condition of conical motion in an ideal state in the reflector coordinate system $O_{46}X_{46}Y_{46}Z_{46}$. (**a**) $a = 1°$, $\omega = 60°/s$; (**b**) $a = 3°$, $\omega = 60°/s$; (**c**) $a = 1°$, $\omega = 180°/s$.

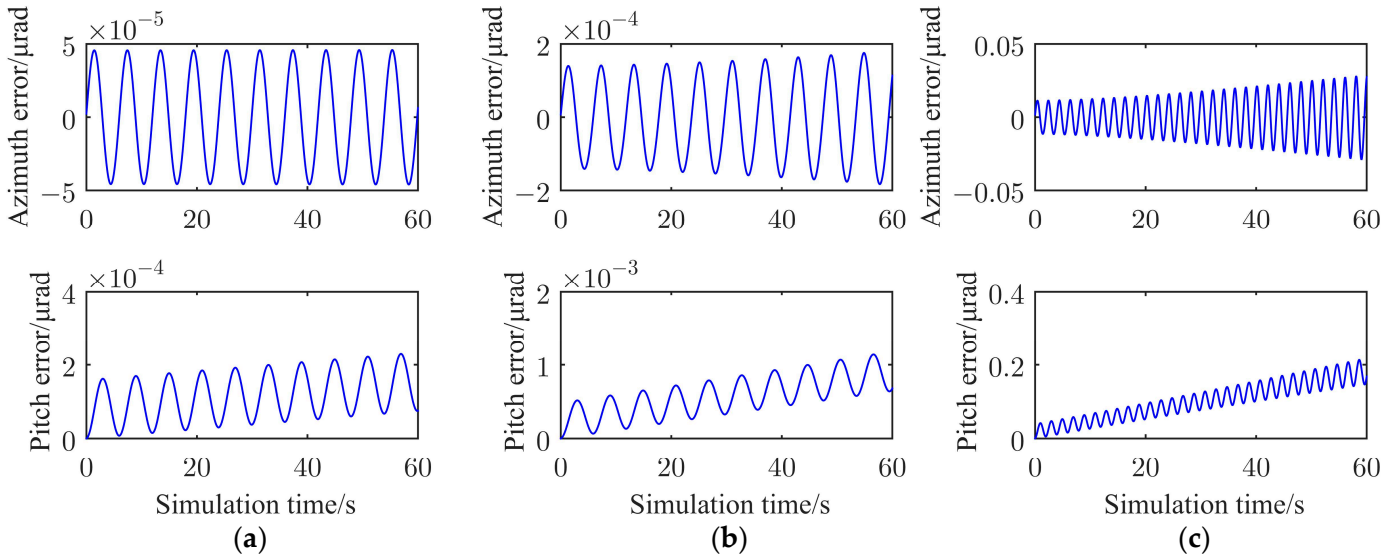

Figure 18. The error curve of the calculation of the indirect numerical calculation method in the reflector coordinate system $O_{46}X_{46}Y_{46}Z_{46}$. (**a**) $a = 1°$, $\omega = 60°/s$; (**b**) $a = 3°$, $\omega = 60°/s$; (**c**) $a = 1°$, $\omega = 180°/s$.

Table 1. The numerical calculation error (μrad) values (1 σ) obtained using the indirect calculation method.

Coordinate Systems of the Reflectors	Attitudes	(a) $a = 1°$, $\omega = 60°/s$	(b) $a = 1°$, $\omega = 180°/s$	(c) $a = 3°$, $\omega = 180°/s$
$O_{41}X_{41}Y_{41}Z_{41}$	Azimuth	4.6×10^{-5}	1.6×10^{-4}	2.0×10^{-2}
	Pitch	1.8×10^{-4}	5.9×10^{-4}	6.3×10^{-2}
$O_{42}X_{42}Y_{42}Z_{42}$	Azimuth	4.6×10^{-5}	1.7×10^{-4}	2.7×10^{-2}
	Pitch	1.5×10^{-4}	6.9×10^{-4}	1.8×10^{-1}
$O_{43}X_{43}Y_{43}Z_{43}$	Azimuth	4.6×10^{-5}	2.0×10^{-4}	4.4×10^{-2}
	Pitch	1.3×10^{-4}	1.2×10^{-3}	2.9×10^{-1}
$O_{44}X_{44}Y_{44}Z_{44}$	Azimuth	4.6×10^{-5}	2.5×10^{-4}	5.2×10^{-2}
	Pitch	1.5×10^{-4}	1.3×10^{-3}	3.2×10^{-1}
$O_{45}X_{45}Y_{45}Z_{45}$	Azimuth	4.6×10^{-5}	2.3×10^{-4}	4.5×10^{-2}
	Pitch	2.1×10^{-4}	1.4×10^{-3}	3.1×10^{-1}
$O_{46}X_{46}Y_{46}Z_{46}$	Azimuth	4.6×10^{-5}	1.8×10^{-4}	2.9×10^{-2}
	Pitch	2.3×10^{-4}	1.1×10^{-3}	2.1×10^{-1}

As can be seen in Table 1, the numerical calculation errors of the attitudes of the LOS of the reflectors were similar in the six reflector coordinate systems. The comprehensive calculation precision in the azimuth and pitch of the attitudes of the LOS of the six reflectors for the conical motion (a) was above 10^{-3} μrad, for the conical motion (b) was over 10^{-2} μrad, and for the conical motion (c) was higher than 0.2 μrad.

Finally, the attitudes of the LOS of the stated six reflectors are directly numerically solved by the angular velocity of the MEMS gyros, and the numerical solution curves of the six LOS attitudes are presented in Figure 19.

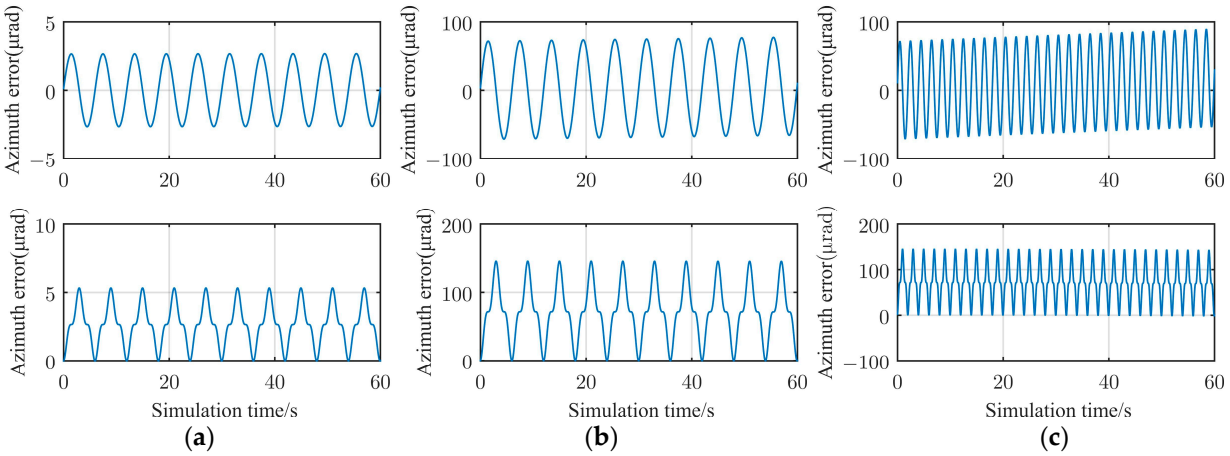

Figure 19. The error curve of the calculation of the direct numerical calculation method. (**a**) $a = 1°$, $\omega = 60°/s$; (**b**) $a = 3°$, $\omega = 60°/s$; (**c**) $a = 1°$, $\omega = 180°/s$.

As shown in Figure 19, the calculation error curves of the attitudes of the LOS of the stated six reflectors were identical regardless of reflector position. The calculation error for the attitudes of the LOS increased with the increments in the cone angle a and the angular velocity ω. The calculation error values are listed in Table 2.

Table 2. The numerical calculation error (μrad) value (1 σ) obtained using the direct calculation method.

Conical Motions.	Attitudes	Calculation Error (μrad)
(a) $a = 1°$, $\omega = 60°/s$	Azimuth	2.7
	Pitch	5.3
(b) $a = 3°$, $\omega = 60°/s$	Azimuth	77.3
	Pitch	145.4
(c) $a = 3°$, $\omega = 180°/s$	Azimuth	89.4
	Pitch	145.6

As observed from Table 2, the comprehensive calculation precision for the conical motion (a) was above 5.3 μrad, for the conical motion (b) was over 145.4 μrad, and for the conical motion (c) was higher than 145.6 μrad. In comparison to the direct calculation method, the indirect calculation method improved the calculation precision by 3, 5, and 3 orders of magnitude in the stated three conical motions, respectively.

For long-distance laser communication, it is theoretically required that LOS stabilization accuracy cannot exceed 10 μrad and even 5 μrad. The factors influencing the stability accuracy of a coarse tracking control system include errors due to MEMS gyro noise and drift, errors due to shaft vibration, an unbalanced moment error, and a dynamic lag error, while there is quite limited space for optimization of these errors. Because of the manufacturing capacity, stabilization accuracy can only reach 20~30 μrad. In order to meet the required LOS stabilization accuracy, as the adjustment compensation in the coarse tracking system, the LOS attitude should have a resolution error as small as possible. The figures show that the resolution accuracy error in the LOS attitude obtained with the indirect method is less than 0.32 μrad, and the influence on LOS stabilization accuracy is less than 1.6%. The resolution accuracy error of the LOS attitude obtained with the direct method is more than 5.3 μrad, and the influence on stabilization accuracy is more than 17.7%, which has a strong influence on LOS stabilization accuracy.

5. Conclusions

In laser communication networking, when multi-address transceivers are mounted with multi-reflectors without 2:1 transmissions, an intrinsic problem of doubled optical

coupling effect between the LOS and the reflectors arises during the rotation of the reflectors. If the angular velocity measured using gyros has to be used for calculating and renewing the attitudes of the LOS, a novel numerical calculation model is required. As has been recognized, the calculation method for the attitudes of the LOS of the reflectors with 2:1 transmissions may also be used for calculating that for the reflectors without 2:1 transmissions. Therefore, a Snell transformation matrix that transforms the reflectors' attitudes into the attitudes of the LOS was created in the present study based on the numerical calculation of the reflectors' attitudes, such that the numerical calculation of the attitudes of the reflectors without 2:1 transmissions could be obtained indirectly. Furthermore, a transformation matrix was established for the multi-reflector coordinate systems. In this manner, the attitudes of the LOS of multi-reflectors were calculated numerically.

The simulation results confirmed that this indirect calculation method applies to calculating the LOS attitudes of reflectors without 2:1 transmissions in any position with high precision. This shows that this method can eliminate the double optical coupling effect. In order to make the simulation close to the real environment, we choose the worst cone motion and added many parameters to simulate realistic experimental conditions. The simulation process and the simulation results can illustrate the effectiveness and superiority of the method in the paper.

Due to the limitation in indoor experimental conditions, this method has not been verified by experiments. The LOS stabilization experiment will be carried out as a future work with the implementation of long-distance laser communication network equipment.

As the requirement for integrated and large-scale development of laser communication networking increases, a large number of reflectors without 2:1 transmissions could be applied to multi-address transceivers. This would increase the quantity and position requirements of the reflectors. In this scenario, the numerical calculation method proposed in the present study would prove to be highly valuable for space laser communication networking.

Author Contributions: L.Z. contributed to the overall study design and analysis; L.W. wrote the whole paper and compiled the whole program; L.M. provided technical support and revised the manuscript. L.W. and Y.B. conducted the simulations, the subsequent data analysis and review; L.Z. and L.W. reviewed and edited the paper. All authors have read and agreed to the published version of the manuscript.

Funding: This research was funded by the Joint Funds of the National Natural Science Foundation of China, grant number U2141231; and the Major Key Project of PCL, grant number PCL2021A03-1.

Data Availability Statement: All data generated and analyzed during this study are included in this article.

Conflicts of Interest: The authors declare no conflict of interest.

References

1. Wang, C.; Zhang, T.; Tong, S.; Li, Y.; Jiang, L.; Liu, Z.; Shi, H.; Liu, J.; Jiang, H. Pointing and tracking errors due to low-frequency deformation in inter-satellite laser communication. *J. Mod. Opt.* **2019**, *66*, 430–437. [CrossRef]
2. Chaudhry, A.U.; Yanikomeroglu, H. Laser intersatellite links in a starlink constellation: A classification and analysis. *IEEE Vehic. Technol. Mag.* **2021**, *16*, 48–56. [CrossRef]
3. Li, R.; Lin, B.; Liu, Y.; Dong, M.; Zhao, S. A survey on laser space network: Terminals, links, and architectures. *IEEE Access* **2022**, *10*, 34815–34834. [CrossRef]
4. Chen, S.; Liang, Y.; Sun, S.; Kang, S.; Cheng, W.; Peng, M. Vision, requirements, and technology trend of 6G: How to tackle the challenges of system coverage, capacity, user data-rate and movement speed. *IEEE Wirel. Commun.* **2020**, *27*, 218–228. [CrossRef]
5. Edwards, B.; Randazzo, T.; Babu, N.; Murphy, K.; Albright, S.; Cummings, N.; Ocasio-Perez, J.; Potter, W.; Roder, R.; Zehner, S.A. Challenges, Lessons Learned, and Methodologies from the LCRD Optical Communication System AI&T. In Proceedings of the 2022 IEEE International Conference on Space Optical Systems and Applications (ICSOS), Kyoto City, Japan, 28–31 March 2022; pp. 22–31.
6. Chishiki, Y.; Yamakawa, S.; Takano, Y.; Miyamoto, Y.; Araki, T.; Kohata, H. Overview of optical data relay system in JAXA. In Proceedings of the Free-Space Laser Communication and Atmospheric Propagation XXVIII, San Francisco, CA, USA, 13–18 February 2016; pp. 114–118.

7. Yamakawa, S.; Chishiki, Y.; Sasaki, Y.; Miyamoto, Y.; Kohata, H. JAXA's optical data relay satellite programme. In Proceedings of the 2015 IEEE International Conference on Space Optical Systems and Applications (ICSOS), New Orleans, LA, USA, 26–28 October 2015; pp. 1–3.
8. Zhang, Y.L.; An, Y.; Wang, C.H.; Jiang, L.; Zhan, J.T.; Liu, X.Z.; Jiang, H.L. Research on rotating paraboloid based surface in space laser communication network. *Acta Opt. Sin.* **2015**, *35*, 86–90. [CrossRef]
9. Zhang, T.; Mao, S.; Fu, Q.; Cao, G.; Su, S.; Jiang, H. Networking optical antenna of space laser communication. *J. Laser Appl.* **2017**, *29*, 012013. [CrossRef]
10. Wang, L.; Zhang, L.; Meng, L.; Bai, Y. A calculation method for line-of-sight stable attitude of networked optical transceiver based on depth feedforward neural network. In Proceedings of the 2022 3rd International Conference on Computer Vision, Image and Deep Learning & International Conference on Computer Engineering and Applications (CVIDL & ICCEA), Changchun, China, 20–22 May 2022; pp. 32–35.
11. Kennedy, P.J.; Kennedy, R.L. Direct versus indirect line of sight (LOS) stabilization. *IEEE Trans. Control Syst. Technol.* **2003**, *11*, 3–15. [CrossRef]
12. Hamilton, A. Strapdown optical stabilization system for EO sensors on moving platforms. Design and Engineering of Optical Systems. *SPIE* **1996**, *2774*, 631–645.
13. Mao, Y.; Tian, J.; Ma, J.G. Realization of LOS (Line of Sight) stabilization based on reflector using carrier attitude compensation method. In XX International Symposium on High-Power Laser Systems and Applications 2014. *SPIE* **2015**, *9255*, 1003–1008.
14. Walter, R.E.; Danny, H.; Donaldson, J. Stabilized inertial measurement system (SIMS). Laser Weapons Technology III. *SPIE* **2002**, *4724*, 57–68.
15. Schneeberger, T.J.; Barker, K.W. High-altitude balloon experiment: A testbed for acquisition, tracking, and pointing technologies. Acquisition, Tracking, and Pointing VII. *SPIE* **1993**, *1950*, 2–15.
16. Gilmore, J.P.; Luniewicz, M.F.; Sargent, D. Enhanced precision pointing jitter suppression system. Laser and Beam Control Technologies. *SPIE* **2002**, *4632*, 38–49.
17. Hilkert, J.M. Inertially stabilized platform technology concepts and principles. *IEEE Contr. Syst. Mag.* **2008**, *28*, 26–46. [CrossRef]
18. Hilkert, J.M. A comparison of inertial line-of-sight stabilization techniques using mirrors. In Proceedings of the Acquisition, Tracking, and Pointing XVIII, Orlando, FL, USA, 12–16 April 2004; pp. 13–22.
19. Masten, M.K. Inertially stabilized platforms for optical imaging systems. *IEEE Control. Syst. Mag.* **2008**, *28*, 47–64.
20. Wu, Y.; Litmanovich, Y.A. Strapdown attitude computation: Functional iterative integration versus taylor series expansion. *Gyroscopy Navig.* **2020**, *11*, 263–276. [CrossRef]
21. Zhao, C.; Fan, J.; Liu, N. Simulation Research on Attitude Solution Method of Micro-Mini Missile. *J. Syst. Simul.* **2019**, *31*, 2877–2884. [CrossRef]
22. Wu, S.; Radice, G.; Gao, Y.; Sun, Z. Quaternion-based finite time control for spacecraft attitude tracking. *Acta Astronaut.* **2011**, *69*, 48–58. [CrossRef]
23. Savage, P.G. Strapdown inertial navigation integration algorithm design part 1: Attitude algorithms. *J. Guid. Contr. Dynam.* **1998**, *21*, 19–28. [CrossRef]
24. Shi, K.; Liu, M. Strapdown inertial navigation quaternion fourth-order runge-kutta attitude algorithm. *J. Detect. Contr.* **2019**, *41*, 61–65.
25. Zhang, Z.; Geng, L.; Fan, Y. Performance Analysis of Three Attitude Algorithms for SINS. *Acad. J. Comput. Inform. Sci.* **2022**, *5*, 1–5. [CrossRef]
26. Lee, J.G.; Yoon, Y.J.; Mark, J.G.; Tazartes, D.A. Extension of strapdown attitude algorithm for high-frequency base motion. *J. Guid. Contr. Dynam.* **1990**, *13*, 738–743. [CrossRef]
27. Jiang, Y.F.; Lin, Y.P. Improved strapdown coning algorithms. *IEEE Trans. Aerosp. Electr. Syst.* **1992**, *28*, 484–490. [CrossRef]